J. Inv. Ill-Posed Problems **16** (2008), 381–396

DOI 10.1515 / JIIP.2008.021

A uniqueness result and image reconstruction of the orthotropic conductivity in magnetic resonance electrical impedance tomography

J. Lin

Abstract. The Magnetic resonance electrical impedance tomography (MREIT) is a new medical imaging method combining electrical impedance tomography (EIT) and current injection MRI technique. In this paper, we show the uniqueness in MREIT problem with an orthotropic conductivity under the hypothesis that the ratios of conductivities are known. Based on an effective numerical differentiation method and an approach to detect discontinuity, we also propose an iterative reconstruction algorithm for the orthotropic conductivity reconstruction. The resulting numerical algorithm is accurate and stable against the noise, and numerical examples are made to illustrate the performance of our algorithm.

Key words. MREIT, orthotropic conductivity, uniqueness, reconstruction algorithm.

AMS classification. 65N21.

1. Introduction

The conventional electrical impedance tomography (EIT) is to recover the interior conductivity from measurements of both the voltages and currents on the boundary. To describe more rigorously, let u denote the electrical voltage in a bounded medium $\Omega \subset \mathbb{R}^n$ with conductivity $\underline{\underline{\sigma}} = (\sigma_{i,j})_{n\times n}$ $(n = 2, 3)$, which is symmetric positive definite, then the voltage u inside the domain and on the boundary satisfies

$$\nabla \cdot (\underline{\underline{\sigma}} \nabla u) = 0 \quad \text{in } \Omega, \qquad u = f \quad \text{on } \partial\Omega.$$

The current flux on $\partial\Omega$ is given by $\underline{\underline{\sigma}} \nabla u \cdot \nu$, where ν denotes the outward unit normal to $\partial\Omega$. The task of EIT problem is to determine $\underline{\underline{\sigma}}$ from the so called Dirichlet-to-Neumann map $\Lambda_{\underline{\underline{\sigma}}} : H^{1/2}(\Omega) \to H^{-1/2}(\Omega)$. It is an imaging tool with important applications in medicine, geophysics, environmental sciences and nondestructive testing [7, 12–14]. Many theoretical and numerical approaches have been studied during the last two decades (see [3] and references therein). However, due to the strong nonlinearity and highly ill-posedness of the problem, the conventional EIT can only yield poor resolution conductivity images.

In order to bypass the ill-posedness of the EIT problem, a new imaging technique called the magnetic resonance electrical impedance tomography (MREIT) has been proposed recently to provide high resolution conductivity images by making use of the current density distribution **J** inside the object. Here **J** is obtained by the so called magnetic resonance current density imaging (MRCDI) technique [5]. That is, by mea-

suring the induced magnetic flux density $\mathbf{B}$ due to the injection current g, the internal current density distribution is acquired by $\mathbf{J} = \nabla \times \mathbf{B}/\mu_0$, where μ_0 is the magnetic permeability of free space. The aim of MREIT is to reconstruct the conductivity from some boundary measurements such as the current flux g and the internal current density data $\mathbf{J}$. To describe mathematically, the MREIT problem is to recover the conductivity $\underline{\underline{\sigma}}$ which satisfies the following boundary value problem:

$$\begin{cases} \nabla \cdot (\underline{\underline{\sigma}} \nabla u) = 0 & \text{in } \Omega, \\ \mathbf{J} = -\underline{\underline{\sigma}} \nabla u & \text{in } \Omega, \\ -\underline{\underline{\sigma}} \nabla u \cdot \nu = g & \text{on } \partial\Omega, \end{cases}$$

where $\mathbf{J}$ and g are given. Sometimes, the voltage potential on the boundary is also utilized [9].

There has been much progress in the image reconstruction of the isotropic conductivity in MREIT, both direct and iterative reconstruction algorithms are proposed to provide high solution conductivity images [8–11]. There are also methods which make use of $\mathbf{B}$ directly [15]. Yet all these MREIT techniques have assumed that the conductivity is isotropic, i.e. $\underline{\underline{\sigma}} = \sigma\mathbf{I}$, here $\mathbf{I}$ denotes the identity matrix in $\mathbb{R}^n$ $(n = 2, 3)$. However, most biological tissues' conductivities are known to be anisotropic. Therefore, theoretical and numerical methods need to be studied for clinical applications of MREIT. The uniqueness in the MREIT problem with anisotropic conductivity has not been answered yet as far as we know. Moreover, there has not been an algorithm to reconstruct the anisotropic conductivity images accurately and efficiently.

In many situations the conductivities of bones and muscles can be reasonably assumed to be orthotropic, i.e. $\underline{\underline{\sigma}} = (\sigma_{i,j})_{n\times n}$ with $\sigma_{ij} = 0$ off the diagonal. The goal of this paper is to present a uniqueness result as well as an accurate reconstruction algorithm for MREIT with such form of conductivity. Under the hypothesis that the ratios between σ_{ii} are known, that is

$$\underline{\underline{\sigma}} = \begin{pmatrix} \sigma & 0 \\ 0 & \kappa\sigma \end{pmatrix} \tag{1.1}$$

with known function κ in two dimensions, we show that the conductivity is uniquely determined if two currents are injected. It should be mentioned that our uniqueness result also holds in three dimensions (see Section 2.1 for theories in more general cases), we just give the definition in $\mathbb{R}^2$ so as to keep our descriptions simple and clear. It should also be pointed out that the uniqueness result presented here is a generalization of the result proposed in [10], where the author presented a uniqueness result for an isotropic MREIT problem, that is $\kappa = 1$ in (1.1), while we set κ as an arbitrary function with some smooth assumption. We would also like to point out that the current density $\mathbf{J}$ is assumed to be given here, which is different from [10]. There less information is needed, i.e, only $|\mathbf{J}|$ is given. This is natural, since when the conductivity σ is a scalar, σ can be retrieved by $\sigma = |\mathbf{J}|/|\nabla u|$. However, this is not valid if the conductivity is a matrix. We also generalize the iterative approach in [10] for the image reconstruction of the orthotropic conductivity. However, during each iteration, we

apply an effective numerical differentiation method introduced in [16] to compute the gradient of the voltage u inside the object. This is totally different from conventional MREIT algorithms, in which the finite difference scheme is a common choice due to its simplicity of implementation. Badly, it is well known that such simplicity would bring a disaster when the grid size is too small [6]. Thus we need a new numerical differentiation method in the reconstruction algorithm to overcome this difficulty. Numerical examples show that [16] is hopeful in dealing with such difficulty. It can also be seen from the numerical tests that our reconstruction algorithm is convergent and accurate, and it is also stable against the noise.

The organization of the paper is as follows. In Section 2, we formulate the MREIT problem mathematically and present the unique result. In Section 3, we describe the reconstruction algorithm in detail, numerical examples are also presented to show the performance of our algorithm. Some concluding remarks are given in Section 4.

2. Uniqueness in the orthotropic MREIT problem

In order to keep our descriptions clear, we formulate the problem in two dimensions. The orthotropic MREIT problem is described as follows. You may refer to [10] for a similar description.

Let $\Omega \subset \mathbb{R}^2$ be a connected and bounded domain with C^2-boundary $\partial\Omega$. It represents a electrically conducting object which has orthotropic conductivity

$$\underline{\underline{\sigma}} = \begin{pmatrix} \sigma & 0 \\ 0 & \kappa\sigma \end{pmatrix}.$$

It is assumed here that $\kappa > 0$ is a known function in $C^1(\bar{\Omega})$ representing the ratio between the conductivities, $\sigma \in C^1(\bar{\Omega})$ and it is strictly positive. Therefore, only σ is unknown in the orthotropic conductivity $\underline{\underline{\sigma}}$.

The injection currents g is applied through a pair of electrodes P and Q attached at the boundary (see Figure 1). Assuming that each electrode is a disk with radius ϵ, we can express the injection current approximately by

$$g(x) = g[\epsilon, P, Q](x) = \begin{cases} 1/(\pi\epsilon^2) & \text{on } \{\, |x-P| < \epsilon\} \cap \partial\Omega \\ -1/(\pi\epsilon^2) & \text{on } \{\, |x-Q| < \epsilon\} \cap \partial\Omega \\ 0 & \text{elsewhere.} \end{cases} \tag{2.1}$$

For more information about injection current, please refer to [10] and references therein. With the current g, the internal current density $\mathbf{J} = -\underline{\underline{\sigma}}\nabla u$ is divergence free and satisfies the boundary condition $\mathbf{J}\cdot\nu = -\underline{\underline{\sigma}}\nabla u\cdot\nu = g$ on $\partial\Omega$ according to the Maxwell equations. That is

$$\nabla\cdot(\underline{\underline{\sigma}}\nabla u) = 0 \quad \text{in } \Omega, \qquad -\underline{\underline{\sigma}}\nabla u\cdot\nu = g \quad \text{on } \partial\Omega.$$

Here u denotes the voltage potential inside the object Ω and ν is the outward unit normal to $\partial\Omega$ here and henceforth. In MREIT, it is assumed that current density $\mathbf{J}$ is measured using MRCDI technique [5].

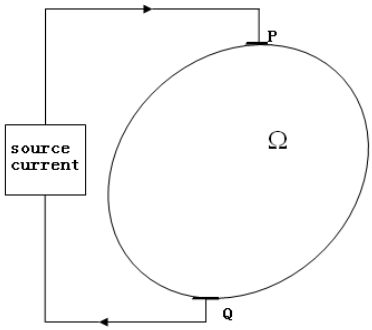

Figure 1. Current is applied through a pair of electrodes P and Q attached at the boundary

We suppose that two currents $g_i = g[\epsilon, P, Q_i]$ $(i = 1, 2)$ are injected sequently, the corresponding current densities $\mathbf{J}^1$ and $\mathbf{J}^2$ are measured. It is assumed here that $u_i(\xi_0) = 0$, where $\xi_0 \in \partial\mathbf{\Omega}$ is an arbitrary point except for P, Q_1 and Q_2. We also apply the normalization of the conductivity with $\sigma(\xi_0) = 1$ in order to fix scaling uncertainty [10]. Coupled with Maxwell equations, the orthotropic MREIT problem can be formulated as follows:

Given the conductivities ratio κ, internal current densities $\mathbf{J}^1, \mathbf{J}^2$, and boundary current fluxes g_1, g_2, to recover the conductivity σ in $\underline{\underline{\sigma}} = \begin{pmatrix} \sigma & 0 \\ 0 & \kappa\sigma \end{pmatrix}$ from the coupled system

$$\begin{cases} \nabla \cdot (\underline{\underline{\sigma}} \nabla u_i) = 0 & \text{in } \mathbf{\Omega}, \quad i = 1, 2, \\ \mathbf{J}^i = -\underline{\underline{\sigma}} \nabla u_i & \text{in } \mathbf{\Omega}, \quad i = 1, 2, \\ -\underline{\underline{\sigma}} \nabla u_i \cdot \nu = g_i & \text{on } \partial\mathbf{\Omega}, \quad u_i(\xi_0) = 0,\ \sigma(\xi_0) = 1. \end{cases} \tag{2.2}$$

Now we proceed to state our uniqueness result in the following theorem.

Theorem 2.1. *Suppose that P, Q_1 and Q_2 are three different points on $\partial\mathbf{\Omega}$, two current fluxes $g_1 = g[\epsilon, P, Q_1]$ and $g_2 = g[\epsilon, P, Q_2]$ are defined by (2.1), the corresponding current densities $\mathbf{J}^1$, $\mathbf{J}^2$ are given. Let (u_1, u_2, σ) and $(\tilde{u}_1, \tilde{u}_2, \tilde{\sigma})$ be two pairs of solutions for the system (2.2) with positive conductivities $\sigma, \tilde{\sigma} \in C^1(\mathbf{\Omega})$, then we have $u_1 = \tilde{u}_1$, $u_2 = \tilde{u}_2$ and $\sigma = \tilde{\sigma}$.*

Before proving this theorem we need the following lemma.

Lemma 2.2. *Assume $\sigma \in C^1(\bar{\Omega})$ is strictly positive and $g_i = g[\epsilon, P, Q_i]$ are defined by* (2.1) $(i = 1, 2)$. *If (u_1, u_2) is a pair of solution for the system* (2.2), *then*

$$\nabla u_1 \times \nabla u_2 \neq 0 \quad \textit{in } \Omega. \tag{2.3}$$

Proof. By the smooth assumption of σ, we have $u_i \in C^1(\Omega) \cap C(\bar{\Omega})$. Suppose that there exits a point $x_0 \in \Omega$ such that $\nabla u_1(x_0) \times \nabla u_2(x_0) = 0$, then there exit non-zero constants c_1 and c_2 such that

$$c_1 \nabla u_1(x_0) + c_2 \nabla u_2(x_0) = 0. \tag{2.4}$$

We define a new function $v = c_1 u_1 + c_2 u_2$. It is easy to verify that v satisfies $\nabla \cdot (\underline{\underline{\sigma}} \nabla v) = 0$ with Neumann boundary $-\underline{\underline{\sigma}} \nabla v \cdot \nu = g = c_1 g_1 + c_2 g_2$. Since g_i is defined by (2.1), therefore, the boundary $\partial\Omega$ can be split into two arcs Γ_1 and Γ_2 such that $g \geq 0$ on Γ_1 and $g \leq 0$ on Γ_2. Then by the index theory of critical points of elliptic partial differential equations in divergence form ([1], [2]), we can conclude that $\nabla v(x) \neq 0$ for all $x \in \Omega$, which contradicts (2.4) by the definition of v. Therefore, $\nabla u_1 \times \nabla u_2 \neq 0$ in Ω. □

Lemma 2.2 plays a significant role in our proof of the uniqueness result, which we now give in the following.

Proof of Theorem 2.1. Since for each i, $\underline{\underline{\sigma}} \nabla u_i = -\mathbf{J}^i$ in Ω (i=1,2), so does

$$\nabla \times (\underline{\underline{\sigma}} \nabla u_i) = -\nabla \times \mathbf{J}^i. \tag{2.5}$$

For simplicity, we denote $-\nabla \times \mathbf{J}^i$ by $\left[H_x^i, H_y^i, H_z^i\right]^T$. Note that the problem we deal with is two dimensional and $\underline{\underline{\sigma}} = \begin{pmatrix} \sigma & 0 \\ 0 & \kappa\sigma \end{pmatrix}$. So we can rewrite the left side of (2.5) as

$$\left[\ 0,\ \ 0,\ \ (\kappa - 1)\sigma \frac{\partial^2 u_i}{\partial x\, \partial y} + \kappa \frac{\partial \sigma}{\partial x} \frac{\partial u_i}{\partial y} - \frac{\partial \sigma}{\partial y} \frac{\partial u_i}{\partial x} + \sigma \frac{\partial \kappa}{\partial x} \frac{\partial u_i}{\partial y}\right]^{\top}.$$

Thus

$$\begin{aligned} H_x^i &= 0, \qquad H_y^i = 0, \\ H_z^i &= (\kappa - 1)\sigma \frac{\partial^2 u_i}{\partial x\, \partial y} + \kappa \frac{\partial \sigma}{\partial x} \frac{\partial u_i}{\partial y} - \frac{\partial \sigma}{\partial y} \frac{\partial u_i}{\partial x} + \sigma \frac{\partial \kappa}{\partial x} \frac{\partial u_i}{\partial y}. \end{aligned} \tag{2.6}$$

On the other hand, by $\underline{\underline{\sigma}} \nabla u_i = -\mathbf{J}^i = -[J_x^i, J_y^i]^T$, we have

$$\frac{\partial^2 u_i}{\partial x \partial y} = \frac{J_x^i}{\sigma^2} \frac{\partial \sigma}{\partial y} - \frac{1}{\sigma} \frac{\partial J_x^i}{\partial y}, \qquad \frac{\partial u_i}{\partial x} = -\frac{J_x^i}{\sigma}, \qquad \frac{\partial u_i}{\partial y} = -\frac{J_y^i}{\kappa\sigma}.$$

Therefore,

$$\begin{aligned} H_z^i &= (\kappa - 1)\sigma\Big(\frac{J_x^i}{\sigma^2} \frac{\partial \sigma}{\partial y} - \frac{1}{\sigma} \frac{\partial J_x^i}{\partial y}\Big) - \frac{\partial \sigma}{\partial x} \frac{J_y^i}{\sigma} + \frac{\partial \sigma}{\partial y} \frac{J_x^i}{\sigma} - \frac{\partial \kappa}{\partial x} \frac{J_x^i}{\kappa} \\ &= (1 - \kappa) \frac{\partial J_x^i}{\partial y} + \kappa \frac{\partial \sigma}{\partial y} \frac{J_x^i}{\sigma} - \frac{\partial \sigma}{\partial x} \frac{J_y^i}{\sigma} - \frac{\partial \ln \kappa}{\partial x} J_x^i. \end{aligned}$$

The formula above can be rearranged as

$$H_z^i + (\kappa - 1)\,\frac{\partial J_x^i}{\partial y} + \frac{\partial \ln \kappa}{\partial x}\,J_x^i = \kappa\,\frac{\partial \ln \sigma}{\partial y}\,J_x^i - \frac{\partial \ln \sigma}{\partial x}\,J_y^i. \tag{2.7}$$

Similarly, for $\tilde{\sigma}$ we obtain

$$H_z^i + (\kappa - 1)\,\frac{\partial J_x^i}{\partial y} + \frac{\partial \ln \kappa}{\partial x}\,J_x^i = \kappa\,\frac{\partial \ln \tilde{\sigma}}{\partial y}\,J_x^i - \frac{\partial \ln \tilde{\sigma}}{\partial x}\,J_y^i. \tag{2.8}$$

Subtraction (2.8) from (2.7) yields

$$\kappa\,\frac{\partial}{\partial y}\Big(\ln\frac{\sigma}{\tilde{\sigma}}\Big)J_x^i - \frac{\partial}{\partial x}\Big(\ln\frac{\sigma}{\tilde{\sigma}}\Big)J_y^i = 0,$$

i.e.

$$\kappa\sigma\,\frac{\partial}{\partial y}\Big(\ln\frac{\sigma}{\tilde{\sigma}}\Big)\frac{\partial u_i}{\partial x} - \kappa\sigma\,\frac{\partial}{\partial x}\Big(\ln\frac{\sigma}{\tilde{\sigma}}\Big)\frac{\partial u_i}{\partial y} = 0. \tag{2.9}$$

Since σ and κ are nonzero, we can conclude that

$$\frac{\partial}{\partial y}\Big(\ln\frac{\sigma}{\tilde{\sigma}}\Big)\frac{\partial u_i}{\partial x} - \frac{\partial}{\partial x}\Big(\ln\frac{\sigma}{\tilde{\sigma}}\Big)\frac{\partial u_i}{\partial y} = 0. \tag{2.10}$$

Again note that the problem is two dimensional, therefore

$$\nabla \ln\frac{\sigma}{\tilde{\sigma}} \times \nabla u_i = -\Big[\ 0,\ \ 0,\ \ \frac{\partial}{\partial y}\Big(\ln\frac{\sigma}{\tilde{\sigma}}\Big)\frac{\partial u_i}{\partial x} - \frac{\partial}{\partial x}\Big(\ln\frac{\sigma}{\tilde{\sigma}}\Big)\frac{\partial u_i}{\partial y}\Big]^{\top} = \vec{\mathbf{0}} \quad \text{in } \Omega. \tag{2.11}$$

By Lemma 2.2, we know that $\nabla u_1 \times \nabla u_2 \neq 0$ in Ω. Hence, we can conclude that $\nabla \ln(\sigma/\tilde{\sigma}) = 0$, or $\ln(\sigma/\tilde{\sigma})$ is a constant in Ω by (2.11). According to the assumption that $\sigma(\xi_0) = \tilde{\sigma}(\xi_0) = 1$, we have $\ln(\sigma/\tilde{\sigma}) = 0$. Therefore, $\sigma = \tilde{\sigma}$ in Ω.

Since $\sigma = \tilde{\sigma}$, u_i and $\tilde{u}_i$ are solutions of the same problem (2.2) with the same Neumann data. Hence, $u_i = \tilde{u}_i$ follows from the uniqueness of the Neumann boundary value problem. This completes the proof. □

In fact, the smooth condition on the orthotropic conductivity $\underline{\underline{\sigma}}$ can be relaxed, and the uniqueness result still holds. We state it in detail in the next theorem.

Theorem 2.3. *Suppose that*

$$\underline{\underline{\sigma_0}} = \begin{pmatrix} \sigma_0 & 0 \\ 0 & \kappa_0\sigma_0 \end{pmatrix}, \qquad \underline{\underline{\sigma_m}} = \begin{pmatrix} \sigma_m & 0 \\ 0 & \kappa_m\sigma_m \end{pmatrix}$$

with known ratios κ_0 and κ_m $(m = 1, \ldots, N)$, respectively.

$$\underline{\underline{\sigma}} \in \Big\{\underline{\underline{\sigma_0}}\chi_{\bar{\Omega}\setminus\cup_{m=1}^N \bar{D}_m} + \sum_{m=1}^{N} \underline{\underline{\sigma_m}}\chi_{D_m} \ \Big|\ \sigma_0 \in C^1(\bar{\Omega}\setminus\cup_{m=1}^N D_m),\ \sigma_m \in C^1(\bar{D}_m)\Big\},$$

where χ denotes the characteristic function for a specific domain, $\bar{D}_m \subset \Omega$ has C^2-boundary and $\bar{D}_m \cap \bar{D}_j = \varnothing$ when $m \neq j$. If $\mathbf{J}^1$, $\mathbf{J}^2$, g_1 and g_2 are given, then $\underline{\underline{\sigma}}$ is uniquely determined by the coupled system (2.2)*.*

Proof. Suppose that we have two solutions $\underline{\underline{\sigma}}$ and $\underline{\underline{\tilde{\sigma}}}$. A parallel proof of Theorem 2.1 shows that $\sigma_m/\tilde{\sigma}_m$ is constant in $\bar{D}_m$ and $\sigma_0/\tilde{\sigma}_0$ is constant in $\bar{\Omega}\setminus\cup_{m=1}^N D_m$, which we denote by c_m and c_0 respectively.

We proceed to show $c_m = c_0$. The process is similar to [10], except for that we deal with the orthotropic conductivity here. In fact, if $c_m \neq c_0$, then due to the transmission condition along the boundary ∂D_m, that is

$$\nabla u_i^+(x)\cdot\tau = \nabla u_i^-(x)\cdot\tau \quad \text{if } x\in\partial D_m,$$

where u_i^+ and u_i^- are voltage potentials in inclusion D_m and background $\Omega\setminus\cup_{m=1}^N D_m$ respectively, τ is the unit tangent vector along ∂D_m, we know that ∇u_i must be normal to ∂D_m. Hence ∂D_m is a potential line of u_i, so u_i is constant in D_m due to maximum principle, which means u_i is constant in the entire Ω by unique continuation. However, this contradicts the definition of the boundary current flux g_i. Thus, $c_m = c_0$, the normalization of $\sigma(\xi) = 1$ implies that $c_m = 1$. This completes the proof. □

Remark 2.4. The uniqueness result for orthotropic MREIT problem (2.2) also holds when $\Omega\subset\mathbb{R}^3$ and $\underline{\underline{\sigma}}$ has the form

$$\begin{pmatrix} \sigma & 0 & 0\\ 0 & \kappa_1\sigma & 0\\ 0 & 0 & \kappa_2\sigma, \end{pmatrix} \tag{2.12}$$

where κ_1 and κ_2 are known ratios. Following the lines of proof in Theorem 2.1, we have

$$\begin{aligned} &\frac{\partial}{\partial y}\Big(\ln\frac{\sigma}{\tilde{\sigma}}\Big)\frac{\partial u_i}{\partial z} - \frac{\partial}{\partial z}\Big(\ln\frac{\sigma}{\tilde{\sigma}}\Big)\frac{\partial u_i}{\partial y} = 0,\\ &\frac{\partial}{\partial x}\Big(\ln\frac{\sigma}{\tilde{\sigma}}\Big)\frac{\partial u_i}{\partial z} - \frac{\partial}{\partial z}\Big(\ln\frac{\sigma}{\tilde{\sigma}}\Big)\frac{\partial u_i}{\partial x} = 0,\\ &\frac{\partial}{\partial y}\Big(\ln\frac{\sigma}{\tilde{\sigma}}\Big)\frac{\partial u_i}{\partial x} - \frac{\partial}{\partial x}\Big(\ln\frac{\sigma}{\tilde{\sigma}}\Big)\frac{\partial u_i}{\partial y} = 0, \end{aligned} \tag{2.13}$$

which implies

$$\nabla\ln\frac{\sigma}{\tilde{\sigma}}\times\nabla u_i = 0, \qquad i = 1,2. \tag{2.14}$$

Hence, $\sigma = \tilde{\sigma}$ holds in the entire Ω following the proof in Theorem 2.1.

3. Reconstruction of orthotropic conductivity

3.1. Reconstruction algorithm

Reconstruction algorithm of the anisotropic conductivity is crucial for the clinical application of MREIT, since most biological tissues have anisotropic conductivities. However, there is not an efficient method to provide high resolution images up to now. Direct reconstruction algorithm like one presented in [9] is not available for anisotropic

media since the direction of equipotential line is unavailable. In this section, we develop an iterative algorithm to reconstruct the orthotropic conductivity images, i.e.

$$\underline{\underline{\sigma}} = \begin{pmatrix} \sigma_{11} & 0 \\ 0 & \sigma_{22} \end{pmatrix}.$$

Note here we do not require that the ratios of conductivities are known, as presented in our uniqueness result. All we required for $\underline{\underline{\sigma}}$ is that it is known at one point, say ξ_0, to fix the scaling uncertainty. Our algorithm is a generalization of one proposed in [10]. However, we deal with orthotropic MREIT problem here. On the other hand, during each iteration an effective numerical differentiation method introduced in [16] is applied to compute the gradient of the voltage u inside the object, which will be discussed in Section 3.2. It is more accurate and stable than the finite difference scheme, which causes severe error when the grid size is too small.

We sequently inject two currents g_1 and g_2. Let u_i $(i = 1, 2)$ be the voltage inside object Ω due to each current g_i respectively, then u_i is a solution of the following boundary value problem

$$\begin{cases} \nabla \cdot (\underline{\underline{\sigma}} \nabla u_i) = 0 \quad \text{in } \Omega, \\ -\underline{\underline{\sigma}} \nabla u_i \cdot \nu = g_i \quad \text{on } \partial\Omega, \quad u_i(\xi_0) = 0. \end{cases} \tag{3.1}$$

We now assume that two current densities $\mathbf{J}^i = (J_x^i, J_y^i, J_z^i)^T$ are measured using the MRCDI technique [5]. From the relationship between $\mathbf{J}^i$ and $\underline{\underline{\sigma}}$, i.e. $\mathbf{J}_i = -\underline{\underline{\sigma}} \nabla u_i$, we have

$$\sigma_{11} \frac{\partial u_i}{\partial x} = -J_x^i, \qquad \sigma_{22} \frac{\partial u_i}{\partial x} = -J_y^i,$$

This formula can be rewritten as

$$\begin{bmatrix} \partial u_1/\partial x \\ \partial u_2/\partial x \end{bmatrix} \sigma_{11} = - \begin{bmatrix} J_x^1 \\ J_x^2 \end{bmatrix}, \qquad \begin{bmatrix} \partial u_1/\partial y \\ \partial u_2/\partial y \end{bmatrix} \sigma_{22} = - \begin{bmatrix} J_y^1 \\ J_y^2 \end{bmatrix}. \tag{3.2}$$

Then our iterative algorithm follows the next 5 steps:

Step 1. Initial guess $\underline{\underline{\sigma}}^0 = \mathbf{I}$. Here $\mathbf{I}$ is identity matrix in $\mathbb{R}^2$.

Step 2. For each $n = 0, 1, \ldots$, solve

$$\begin{aligned} &\nabla \cdot (\underline{\underline{\sigma}}^n \nabla u_i^n) = 0 \quad \text{in } \Omega, \quad (i = 1, 2) \\ &-\underline{\underline{\sigma}}^n \nabla u_i^n \cdot \nu = g_i \quad \text{on } \partial\Omega, \quad u_i^n(\xi_0) = 0. \end{aligned} \tag{3.3}$$

Step 3. Apply the numerical differentiation method introduced in Section 3.2 to calculate the partial derivatives of u_i respectively, i.e. $\partial u_i^n/\partial x$ and $\partial u_i^n/\partial y$.

Step 4. If $\|\underline{\underline{\sigma}}^n \nabla u_1^n + \mathbf{J}^1\|_{L^2(\Omega)} + \|\underline{\underline{\sigma}}^n \nabla u_2^n + \mathbf{J}^2\|_{L^2(\Omega)} < \epsilon$, where ϵ is a given tolerance, then the iteration is terminated.

Step 5. Update the orthotropic conductivity using formula

$$\begin{bmatrix} \partial u_1^n/\partial x \\ \partial u_2^n/\partial x \end{bmatrix} \sigma_{11}^{n+1} = - \begin{bmatrix} J_x^1 \\ J_x^2 \end{bmatrix}, \qquad \begin{bmatrix} \partial u_1^n/\partial y \\ \partial u_2^n/\partial y \end{bmatrix} \sigma_{22}^{n+1} = - \begin{bmatrix} J_y^1 \\ J_y^2 \end{bmatrix}. \quad (3.4)$$

followed by a scaling procedure

$$\sigma_{11}^{n+1} = \frac{\sigma_{11}(\xi_0)}{\sigma_{11}^{n+1}(\xi_0)}\, \sigma_{11}^{n+1}, \qquad \sigma_{22}^{n+1} = \frac{\sigma_{22}(\xi_0)}{\sigma_{22}^{n+1}(\xi_0)}\, \sigma_{22}^{n+1}, \quad (3.5)$$

where (3.4) is solved in the least square sense, and $\sigma_{11}(\xi_0)$ and $\sigma_{22}(\xi_0)$ are known conductivities at ξ_0.

During each iteration, we hope to approximate $\underline{\underline{\sigma}}$ by imposing (3.4), which is solved in least-square sense here. On the other hand, procedure (3.5) is applied to fix scaling uncertainty. The stopping criterion comes from the observation that $\left\|\underline{\underline{\sigma}}^n \nabla u_1^n + \mathbf{J}^1\right\|_{L^2(\Omega)} + \left\|\underline{\underline{\sigma}}^n \nabla u_2^n + \mathbf{J}^2\right\|_{L^2(\Omega)}$ decreases monotonically during the iteration process before it reaches a minimum.

3.2. Numerical differentiation and discontinuity detection

During each iteration of reconstruction procedure, when u_i^n is solved numerically from (3.3), we have to compute their partial derivatives numerically in Step 3 before updating the conductivity. As is known, numerical differentiation is an ill-posed problem, which means very small error in u_i^n may cause huge errors in their derivatives. Therefore, an accurate and stable approach of numerical differentiation is crucial to a successful reconstruction of the conductivity. Conventional MREIT reconstruction algorithm usually utilize a finite difference scheme to approximate the derivatives and suitably choose the size of grid. However, it has been shown that the size of the grid should not be too small in a finite difference procedure [6], which means the resolution of reconstructed image will eventually be sacrificed. Moreover, The situation becomes more severe when the object contains inclusions, which is usually the case in practical problems. Another shortcoming of finite difference scheme is lack of the smoothness of resulting approximation functions.

In our algorithm we deal with this numerical differentiation problem by Tikhonov regularization. It was fully studied in [16]. Here we states the theory briefly, you may refer to [16] for details. Suppose $f \in H^2[0,1]$, where $H^2[0,1]$ is the standard sobolev space. $\Delta = \{0 = x_0 < x_1 < \ldots < x_n = 1\}$ is a grid defined on $[0,1]$ with spacing $h_j = x_j - x_{j-1}$ $(j = 1, \ldots, n)$. Given sample data $\tilde{f}_j$ with a level of noise δ, a cost functional is defined by

$$\Phi(g) = \sum_{j=1}^{n-1} \frac{h_j + h_{j+1}}{2} \left(\tilde{f}_j - g(x_j)\right)^2 + \alpha \left\|g''\right\|_{L^2(0,1)}, \quad (3.6)$$

where α is the regularization parameter.

Then the numerical differential problem is converted into finding a minimizer of (3.6) in $H^2[0,1]$. It can be shown that such a minimizer solution is a cubic spline g_* over the grid Δ. Moreover, it has been proved that

$$\|g'_* - f'\|_{L^2(0,1)} \leq \left(2h + 4\alpha^{1/4} + \frac{h}{\pi}\right)\|f''\|_{L^2(0,1)} + h\sqrt{\frac{\alpha}{\delta^2}} + \frac{2\delta}{\alpha^{1/4}}, \tag{3.7}$$

where $h = \max_{1\leq j\leq n} h_j$.

The idea of regularization parameter choice comes from the results in [4], which is based on the conditional stability for ill-posed problems. If we set $\alpha = \delta^2$, then

$$\|g'_* - f'\|_{L^2(0,1)} \leq \left(2h + 4\sqrt{\delta} + \frac{h}{\pi}\right)\|f''\|_{L^2(0,1)} + h + 2\sqrt{\delta}. \tag{3.8}$$

It can be seen from (3.8) that the error $\|g'_* - f'\|_{L^2(0,1)}$ remains of order $O(\sqrt{\delta})$ when $h \to 0$. Hence, the "small grid disaster" of the finite difference scheme is avoided.

It was also proposed in [16] that g''_* can be calculated to obtain detailed information about the discontinuous points of f. This is based on the theory that if f is piecewise continuous and g_* is the minimizer of problem (3.6), then $\|g''_*\|_{L^2(0,1)}$ goes to infinity as $\delta, h \to 0$.

During our implementation, if current is injected on the boundary, we note that current density is piecewise continuous when the conductivity is piecewise smooth. For instance, in the case where some inclusions are contained in the object. Usually, the larger conductivity value one inclusion has, the larger corresponding current density magnitude it has. Therefore, we could apply the method above, i.e., from the information of second derivative of **J**, to distinguish such discontinuities across the boundaries of inclusions. It can be seen from our numerical examples in Section 3.3 that the boundaries of inclusions can be successfully identified.

Suppose that the boundaries of the inclusion are detected, then during each iteration, when u_i^n is solved numerically from (3.3), we try to calculate partial derivatives of u_i^n piecewisely. By finding the natural cubic spline which is the minimizer of problem (3.6) on each subinterval, where u_i^n is smooth, we eventually obtain the partial derivative of u_i^n on the whole interval. This process is illustrated in Figure 2. Suppose that the object contains an inclusion, which we denote by shadowed area in Figure 2, Γ is the boundary of inclusion that has been identified by information of **J**, then we carry the numerical differentiation piecewisely on $[A, B)$, $[B, C]$ and then $(C, D]$ to get a full information of $\partial u_i^n/\partial x$ on $y = y_0$.

3.3. Numerical examples

Numerical simulations are implemented to illustrate the performance of our algorithm. The first numerical test demonstrates the accuracy and convergence behavior of the implementation, the second shows robustness and stability of the method with noisy data.

Consider a rectangular model object $[0,1] \times [0,1]$, which we denote by Ω. Assume that the object contains two inclusions — a disk and an ellipse. The disk is centered

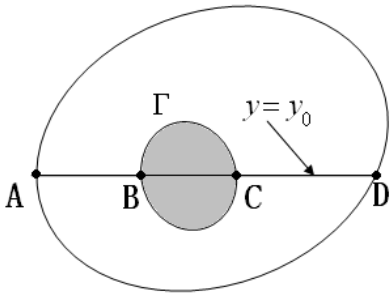

Figure 2. An illustration of numerical differentiation carried piecewisely on $y = y_0$

Region	σ_{11}	σ_{22}
disk	0.40	0.65
ellipse	0.30	0.45
background	0.20	0.30

Table 1. Conductivity values of the model object

in $(0.45, 0.55)$ with the radius 0.15, and the ellipse has the semimajor axis 0.1 and the semiminor axis 0.07, respectively. Both the inclusions and the background material are assumed to be orthotropic, i.e. $\sigma_{ij} = 0$ off the diagonal. The values of diagonal conductivities σ_{11} and σ_{22} are listed in Table 1. Figure 3a and 3b show the corresponding images. To fix scaling uncertainty, the value of conductivity at $(x, y) = (0, 0)$ is supposed to be known in our experiments.

Two currents

$$g_1 = \begin{cases} 5, & \{(0,y) \mid 0 < y < 1\}, \\ -5, & \{(1,y) \mid 0 < y < 1\}, \end{cases} \qquad g_2 = \begin{cases} -5, & \{(x,0) \mid 0 < x < 1\}, \\ 5, & \{(x,1) \mid 0 < x < 1\} \end{cases}$$

are applied sequently on the boundary. In order to generate data simulating $\mathbf{J}^i$ for assumed conductivity and injected currents, standard second order FEM is used to calculate the internal current densities. Figure 4a and 5a visualize the magnitude of internal current densities $|\mathbf{J}^1|$ and $|\mathbf{J}^2|$ respectively.

Example 3.1 (accuracy and convergence). In our first experiment, no noise is added to the simulating data $\mathbf{J}^1$ and $\mathbf{J}^2$. Now we apply the method introduced in Section 3.2 to detect the discontinuities of $|\mathbf{J}^1|$ and $|\mathbf{J}^2|$ inside the object. The detecting results are shown in Figure 4b and 5b. It can be seen that if these two figures are combined, we can successfully identify the boundaries of the inclusions.

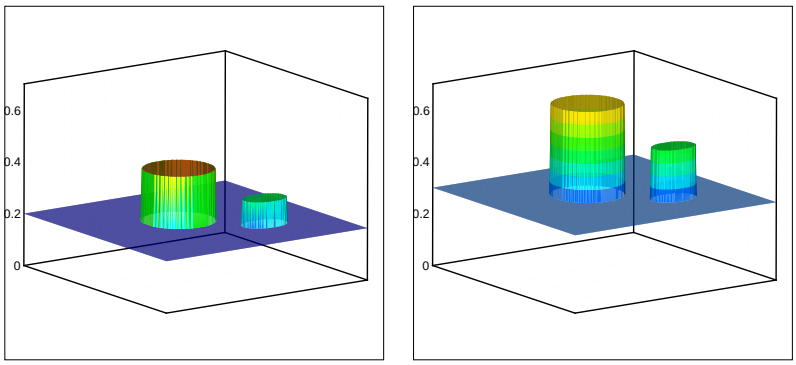

(a) (b)

Figure 3. Images of true conductivities σ_{11} and σ_{22}

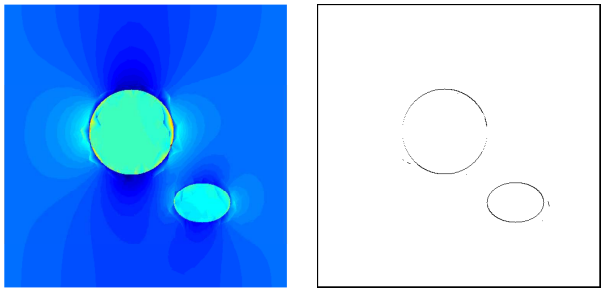

(a) (b)

Figure 4. (a) Magnitude of simulating current density $\mathbf{J}^1$; (b) Identification image

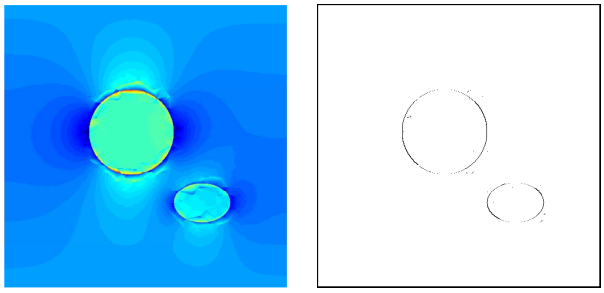

(a) (b)

Figure 5. (a) Magnitude of simulating current density $\mathbf{J}^2$; (b) Identification image

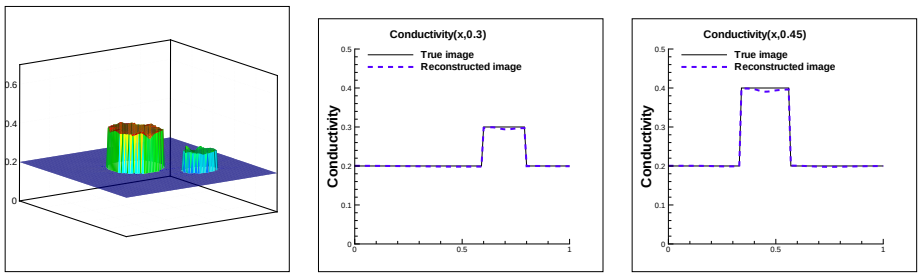

(a) (b) (c)

Figure 6. (a) Reconstructed conductivity image σ_{11}^{rec}; (b) and (c) Cross section value of true and computed conductivity

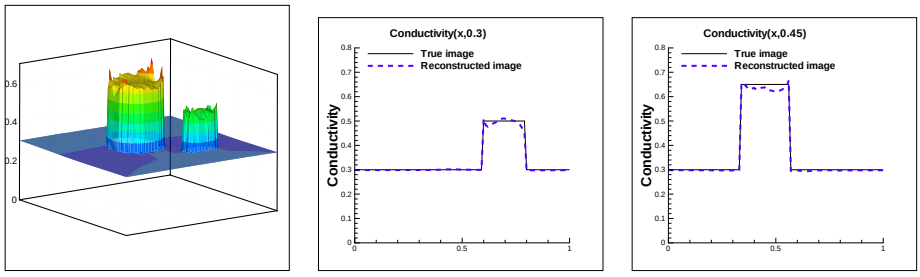

(a) (b) (c)

Figure 7. (a). Reconstructed conductivity image σ_{22}^{rec}; (b) and (c) Cross section value of true and computed conductivity

Figure 6 and Figure 7 show the reconstructed conductivity images σ_{11}^{rec} and σ_{22}^{rec} after 50 iterations. Figure 6a and 7a are surface plots of reconstructed conductivities. The cross section of the conductivity values at $y = 0.3$ and 0.45 are shown in Figure 6b,c and 7b,c respectively. Here dash lines represent the computed conductivities while solid lines are the true values. It can be seen that the proposed algorithm successfully produces the image of the orthotropic conductivities. Not only the boundary of two inclusions are sharply identified, the values of conductivities are comparable to true values, too. We conjecture that the accuracy of our algorithm is mainly due to the approach to detect inclusion boundaries and do numerical differentiation piecewisely.

In Figure 8 we show the convergence behavior of the algorithm, the x-axis represents the number of iterations and y-axis is the relative conductivity error in L^2 norm, i.e. $\|\sigma_{ii}^{\text{true}} - \sigma_{ii}^{\text{rec}}\|_{L^2(\Omega)} / \|\sigma_{ii}^{\text{true}}\|_{L^2(\Omega)}$ with $i = 1$ and 2, respectively. It can be seen from the plot that the errors of reconstructed conductivities decrease quickly during the first 30 iterations and, though the convergence slows down in the following iterations, the errors are still decreasing.

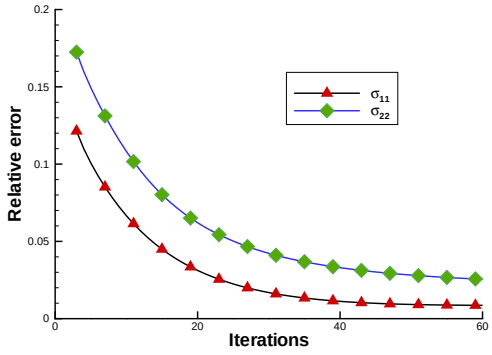

Figure 8. Relative errors of reconstructed conductivities σ_{11}^{rec} and σ_{22}^{rec}

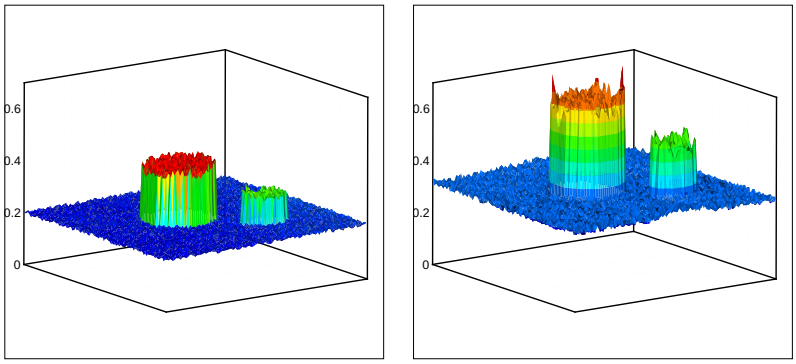

(a) (b)

Figure 9. Reconstructed conductivity images σ_{11}^{rec} and σ_{22}^{rec} with 5% additive noise

Example 3.2 (stability against noise). In order to test the noise tolerance of our algorithm, we add uniformly distributed noise to the simulating data $\mathbf{J}^1$ and $\mathbf{J}^2$. For each pixel, 5% of the magnitude of the corresponding current density component is multiplied by the outcome of a uniform random number generator, which has a range of ± 1, and the result is added to that current density component. The image obtained with the noisy current densities (see Figure 9) indicates that the conductivities can still be successfully reconstructed. Though there is small dent in the image, the boundaries of the inclusions are still sharply identified. We vary the noise level from 1% to 10% and get the corresponding relative errors of the reconstructed conductivities after 30 iterations. The result is illustrated in Figure 10. The x-axis represents the noise level while the y-axis is the relative errors of reconstructed conductivities. It can be seen that the reconstruction errors are almost linearly proportional to noise level, hence our reconstruction method is stable against additive noise.

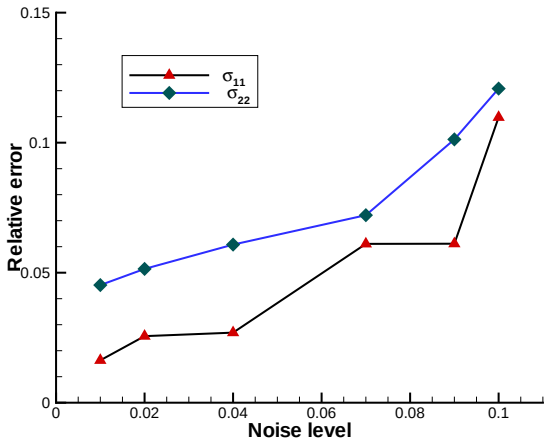

Figure 10. Relative error of reconstructed conductivities with respect to noise level

4. Conclusion

Most previous studies in MREIT assumed isotropy of conductivity. However, numerous biological tissues have anisotropic conductivities, thus we should provide a reconstruction algorithm to handle the anisotropy in imaging techniques. MREIT is promising since it incorporates internal current density measurements.

We proposed a uniqueness result for the orthotropic MREIT problem, assuming that the ratios between the conductivities are known. We also generalize the so called J-substitution method for orthotropic problem. The numerical examples implemented show that this reconstruction algorithm is accurate and convergent, it is also stable against noise.

Numerical differentiation plays a significantly role in reconstruction algorithm. Conventional reconstruction algorithm usually applies the finite difference scheme to compute the gradient of voltage u, which brings large errors when the size of grid is too small. The situation becomes more severe when the object contains inclusions, which is usually the case in practical problems. The numerical differentiation method introduced in [16] is hopeful in dealing with such problems.

For future study, we should concentrate the uniqueness issue in more general cases. On the other hand, convergence of algorithm should be answered rigorously. It is equally important to provide an algorithm directly utilizing z-component of the magnetic field $\mathbf{B}$, instead of using $\mathbf{J}$ directly, since it is not easy to get the full components of $\mathbf{B}$ so as to obtain internal current density by $\mathbf{J} = \nabla \times \mathbf{B}/\mu_0$. We will discuss the nature of $\mathbf{B}$-type MREIT and possible numerical methods for anisotropic problem in future papers.

References

1. G. Alessandrini and R. Magnanini, The index of isolated critical points and solutions of elliptic in the plane. *Ann. Scuola. Norm. Sup. Pisa. Cl. Sci.* **19** (1992), 567–589.
2. G. Alessandrini, Elliptic equations in divergence form, geometric critical point of solutions and Stekloff eigenfunctions. *SIAM J. Math. Anal.* **25** (1994), 1259–1268.
3. L. Borcea, Electrical impedance tomography. *Inverse Problems* **18** (2002), 99–136.
4. J. Cheng and M. Yamamoto, A new strategy for a priori chioce of regularizing parameters in Tikhonov's regularization. *Inverse Problems* **16** (2000), 31–38.
5. H. E. Gamba, D. Bayford, and D. Holder, Measurement of electrical current density distribution in a simple head phantom with magnetic resonance imaging. *Phys. Med. Biol.* **44** (1999), 281–291.
6. M. Hanke and O. Scherzer, Inverse problem light: numercial differentiation. *Am. Math. Mon.* **108** (2001), 512–521.
7. N. D. Harris, A. J. Suggett, D. Barber, and B. Brown, Applications of applied potential tomography (APT) in respiratory medicine. *Clin. Phys. Physiol. Meas.* **8** (1987), 155–165.
8. Y. Z. İder, S. Onart, and W. Lionheart, Uniqueness and reconstruction in magnetic resonance tomography (MR-EIT). *Phy. Meas* **24** (2003), 591–604.
9. O. Kwon, J. Y. Lee, and J. R. Yoon, Equipotential line method for magnetic resonance tomography. *Inverse Problems* **18** (2002), 1–12.
10. Y. J. Kim, O. Kwon, J. K. Seo, and E. J. Woo, Uniqueness and convergence of conductivity image reconstruction in magnetic resonance tomography. *Inverse Problems* **19** (2003), 1213–1225.
11. J. Y. Lee, A reconstruction formula and uniqueness of conductivity in MREIT using two internal injection currents. *Inverse Problems* **20** (2004), 847–858.
12. R. L. Parker, The inverse problem of resistivity sounding. *Geophysics* **142** (1984), 2143–2158.
13. A. Ramirez, W. Daily, B. Binley, D. LaBreque, and D. Roelant, Detection of leaks in underground storage tanks using electrical resistance methods. *J. Environ. Eng. Geophys.* **1** (1996), 189–203.
14. A. Ramirez, W. Daily, D. LaBreque, E. Owen, and D. Chesnut, Monitoring an underground steam injection process using electrical resistance tomography. *Water Resources Res.* **29** (1993), 73–87.
15. J. K. Seo, J. R. Yoon, E. J. Woo, and O. Kwon, Reconstruction of conductivity and current Density images using only one component of magnetic field measurements. *IEEE Trans. Med. Imag.* **50** (2003), 1121–1124.
16. Y. B. Wang, X. Z. Jia, and J. Cheng, A numerical differentiation and its application to reconstruction of discontinuity. *Inverse Problems* **18** (2002), 1461–1476.

Received April 10, 2007; revised December 12, 2007

Author information

J. Lin, School of Mathematical Sciences, Fudan University, Shanghai 200433, China.
Email: linjunsh@msu.edu